A high-resolution oxygen A-band and water vapor band spectrometer

Q.-L. Min, L. C. Harrison, P. Kiedron, and J. Berndt
Atmospheric Sciences Research Center, State University of New York, Albany, New York, USA

E. Joseph
Department of Physics and Astronomy, Howard University, Washington, D.C., USA

Received 26 February 2003; revised 22 September 2003; accepted 3 October 2003; published 17 January 2004.

[1] A prototype high-resolution oxygen A-band and water vapor band spectrometer (HAWS) and new theoretical framework have been developed and demonstrated to study the applicability of photon path length statistics in the remote sensing of clouds, aerosols, and water vapor, particularly in addressing current challenges such as the detection of thin layers of clouds and aerosols especially over surfaces with high albedo, reducing retrieval errors due to the presence of non-spherical particles, and enhancing the vertical resolution of retrieved atmospheric constituents. This work also provides a basis for the application of path length distribution in the development and validation of radiative transfer parameterizations that account for the effects of cloud inhomogeneity. The HAWS successfully achieves an out-of-band rejection of better than 10^{-5}, a resolution of better than 0.5 cm^{-1}, and high signal-to-noise ratio, which are crucial to retrieval of atmospheric information through high-resolution spectrometry in the A-band and water vapor band. A field campaign was conducted to demonstrate the capabilities of HAWS and the new retrieval algorithm at the cloud and radiation testbed at ARM SGP site in Oklahoma, where a comprehensive set of radiometric, passive, and active sensors provide continuous and concurrent measurements of clouds, aerosols, water vapor, and other atmospheric properties. Results show that in the A-band thick and multiple layer clouds significantly enhance the mean and variance of the photon path length distribution, thin cirrus condition produce relatively small mean distribution and variance, and mean path lengths comparable to or smaller than the solar airmass were associated with clear sky cases at large solar zenith angles. The mean path length and variance in the water vapor band differs from that in the A-band due to the spatial inhomogeneity of water vapor amounts, particularly in association with cloud layers. *INDEX TERMS:* 0360 Atmospheric Composition and Structure: Transmission and scattering of radiation; 1640 Global Change: Remote sensing; 0320 Atmospheric Composition and Structure: Cloud physics and chemistry; *KEYWORDS:* cloud, water vapor, photon path length

Citation: Min, Q.-L., L. C. Harrison, P. Kiedron, J. Berndt, and E. Joseph (2004), A high-resolution oxygen A-band and water vapor band spectrometer, *J. Geophys. Res.*, *109*, D02202, doi:10.1029/2003JD003540.

1. Introduction

[2] There are numerous ongoing and planned remote-sensing efforts to characterize the key properties of clouds, aerosol, and water vapor to understand earth climate and predict how it may change due to natural and anthropogenic influences. Detailed knowledge of the important roles these constituents play in the earth energy and hydrological cycles is required to properly characterize climate forcing mechanisms and quantify the response of the climate system to these mechanisms. For example, positive feedback associated with redistribution of water vapor from an increase of surface temperature is the driving mechanism behind the climate warming results of most GCM experiments, but recent studies based on space-borne observations suggest that the net feedback maybe less straight forward than suggested by GCMs and may depend on complex interdependences among surface temperature, upper-level cloudiness, and water vapor distribution in the free troposphere not represented in current GCM parameterizations [*Houghton et al.*, 2001]. Resolving such gaps in present understanding of the hydrological cycle and how it couples with radiative transfer requires concurrent observations of water vapor and clouds at the same location and on the same spatial scales. The present paper reports an effort to obtain high resolution measurements of photon path length distribution in the 760 nm oxygen A-band and 820 nm water vapor band. These data allow us to study where and how water vapor absorbs solar radiation as modulated by clouds and radiation transfer through inhomogeneous clouds. We

0148-0227/04/2003JD003540$09.00

believe these data will contribute to the effort in understanding how cloud-water vapor interactions, will respond to and feedback upon climate change, and in the latter case, will enable explicit treatment of photon path length distribution in the radiative schemes of climate models, and retrieval of the vertical structure of clouds and aerosols.

[3] The interest in photon path length distribution as a tool in remote sensing has a long history [*Grechko et al.*, 1973; *Fischer and Grassl*, 1991; *Fischer et al.*, 1991; *O'Brien and Mitchell*, 1992; *Harrison and Min*, 1997; *Pfeisticker et al.*, 1998; *Veitel et al.*, 1998; *Min and Harrison*, 1999; *Stephens and Heidinger*, 2000; *Heidinger and Stephens*, 2000; *Portmann et al.*, 2001; *Min et al.*, 2001]. Recently it has been revived as part of the effort to resolve some of the more difficult challenges such as the treatment of radiative transfer through inhomogeneous clouds in climate models, retrieval of clouds and aerosols over highly reflecting surfaces, or the problem described above of simultaneous observation of clouds and water vapor as a means of improving understanding of cloud-water vapor interactions [*Min and Clothiaux*, 2003]. The concept of photon path length distribution has also been investigated in active lidar observations [*Davis et al.*, 1999; *Love et al.*, 2001]. Photon path length distribution is commonly a hidden property of standard radiation transfer models, controlled by spatial distributions of scattering and absorption. It is intimately linked to the absorption process in the atmosphere, and distributions in the near-IR region are very representative of the shortwave region as a whole. The principle of equivalence allows conclusions to be drawn about radiative properties of the atmosphere at any other nearby wavelength from a photon path length distribution measurement in one wavelength band [*Irvine*, 1964, 1967; *van de Hulst*, 1980; *Partain et al.*, 2000], since the scattering properties of cloud and aerosol vary slowly and predictably with wavelength. In the case where the radiation arrives from multiple paths the equivalence theorem states:

$$\frac{I(\lambda)}{I(\lambda_0)} = \int_0^\infty e^{-\chi(\lambda)\bullet l} P(l)dl,$$

where $I(\lambda)$ is the radiance at a wavelength λ, $I(\lambda_0)$ is the radiance at a conservative scattering wavelength λ_0, $\chi(\lambda)$ is the product of the absorption cross-section per unit mass times absorber density, and l is the atmospheric path length. The path length probability density function (PDF) in the multiple-path case is expressed as $P(l)$. In theory, the photon path length PDF can be obtained from a resolved absorption line shape by taking the inverse Laplace transform. In practice there are both inversion and observational limitations. The O_2 A-band is used for assessing path length distribution because it offers important practical advantages: the vertical profile of O_2 is well known; no other known absorbers interfere with the O_2 A-band absorption; and the O_2 A-band provides a number of absorption lines covering a suitable dynamic range of opacities in the atmosphere. For assessing path length distribution associated with water vapor, the 820 and 940 nm bands are ideal because of their close proximity to the A-band. The consequence is that photon path length information derived from the A-band can be applied to the water vapor band at 820 or 940 nm without any further assumptions, and to study cloud-water vapor interaction.

Figure 1. The photo of the HAWS taken at the ARM SGP site during the field campaign.

[4] This paper specifically reports on the development of a prototype high resolution A-band and water vapor band spectrometer (HAWS), a theoretical framework for the HAWS algorithm, and results from a field experiment to demonstrate the capability of the spectrometer-algorithm system. The design accomplishments of the HAWS, in particular, is unprecedented in that the instrument is able to achieve out-of-band rejection of better than 10^{-5}, a resolution of better than 0.5 cm^{-1}, and high signal-to-noise ratio. Results of the field campaign conducted in June 2001 at the Atmospheric Radiation Measurement Southern Great Plains site in Oklahoma demonstrate the field operations of the HAWS, and moreover demonstrate the importance of the design features in obtaining photon path length statistics capable of discriminating among different cloud geometry and sky scenes, and the rich scientific value of combined A-band and water vapor band measurements. The paper is organized as follows: section 2 describes the HAWS, the importance of high resolution and out of band rejection and the algorithm; section 3 reports results of the field campaign; and section 4 discusses and summarizes the results.

2. Instrument Design and Algorithm Development

[5] The spectrometer, shown in Figure 1, was developed by modifying an existing Acton grating monochrometer. Operating the Acton as a spectrograph requires one minute to swing between the A-band and water vapor band (measurements are not taken simultaneously at both bands). The spectrometer was also equipped with a thermoelectric

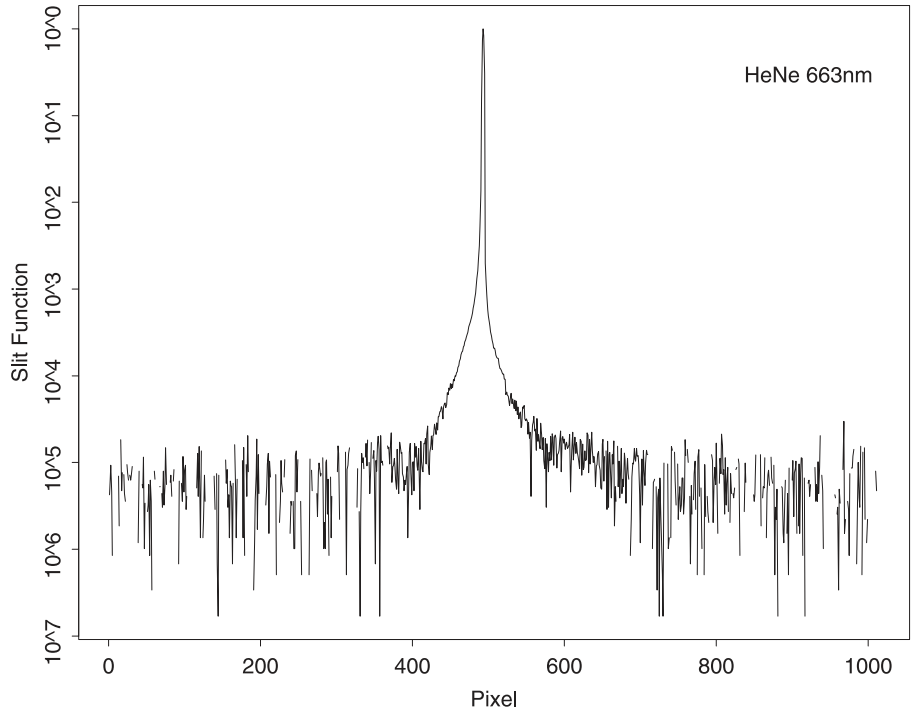

Figure 2. Slit-scattering function of oxygen A-band and water vapor band spectrometer (HAWS).

cooled charge coupled device (CCD) array (256 × 1024) and electronics that was borrowed from a rotating shadowband spectroradiometer (RSS). The CCD area of the system is cooled to 5 C to reduce readout noise, and flushed with dry air while operating to eliminate water condensation on the CCD. The 1200 grooves per mm (g/mm) grating was replaced with an 1800 g/mm grating to increase dispersion and resolution. A telescope with a field of view (FOV) of 11° and an alt-azimuth tracker to automate sun tracking was used to observe the solar direct beam for both bands. This observation will serve as a way to calibrate the instrument and to determine transmittance for the retrievals. A fiber optic bundle coupled the telescope to the instrument fore-optics. The fore-optics has an additional shutter that is used to attenuate the signal while direct beam measurements are taken. The whole system is housed in an enclosure to maintain temperature stability and to protect it from the elements.

2.1. Importance of High Resolution, Out-of-Band Rejection, and Signal-to-Noise Ratio

[6] In order to make useful inversions from absorption spectroscopy it is crucial to have low stray light contribution to the measurement; the Out-of-Band (OOB) rejection criterion becomes more stringent as resolution is improved [*Harrison and Min*, 1997; Q. Min, and L. C. Harrison, Retrieval of atmospheric optical depth profile from downward-looking high-resolution O2 A-band measurements: Optically thin conditions, manuscript submitted to *Journal of Atmospheric Science*, 2003, hereinafter referred to as Min and Harrison, submitted manuscript, 2003]. To understand the impact of instrument specification on the information content, Min and Harrison (submitted manuscript, 2003) constructed a linear inversion kernel for TOA radiance based on the single-scattering approximation. Sensitivity studies show that the most dominant contributions for observed radiance are due to the single and/or lower-order scattering for small oxygen absorption coefficient of k and single scattering for large k. A linear set of equations can be written for the single scattering component (and the multiple scattering component can be treated as a perturbation), particularly under clear-sky conditions. Singular Value Decomposition of the inversion kernels is used at various resolutions and OOB rejections to understand the consequences of instrument specification on potential retrievals. As discussed in *Stephens and Heidinger* [2000] and Min and Harrison (submitted manuscript, 2003), a system with Signal-to-Noise Ratio (SNR) of 100:1 and OOB of 10^{-3} has four independent pieces of information. The following results show that these goals are achievable. Figure 2 shows the slit-scattering function measured against the 643 nm HeNe laser line, to demonstrate achieved OOB rejections of better than 10^{-5} with resolution of 0.025 nm (better than 0.5 cm^{-1}). The SNR depends on both readout and Poisson noise terms. When the signal is weak (near the absorption line center), the readout noise dominates. Given the dynamic range of the measurements, our sampling strategy was to take three short exposures (optimized on sky conditions), then averaged them. For the case shown in Figure 3, each expose was 0.25 second and 7.2 second apart at 18:51 (UTC) on 20 June 2001. The minimum SNR is 64 and 75 in R and P branches, respectively (we only used the P branch for our retrieval). However, signal strength also depends on solar zenith angle and sky conditions, and so does the SNR.

[7] Figure 4 shows measured spectra at oxygen A-band and 820 nm water vapor band obtained at the ARM site on

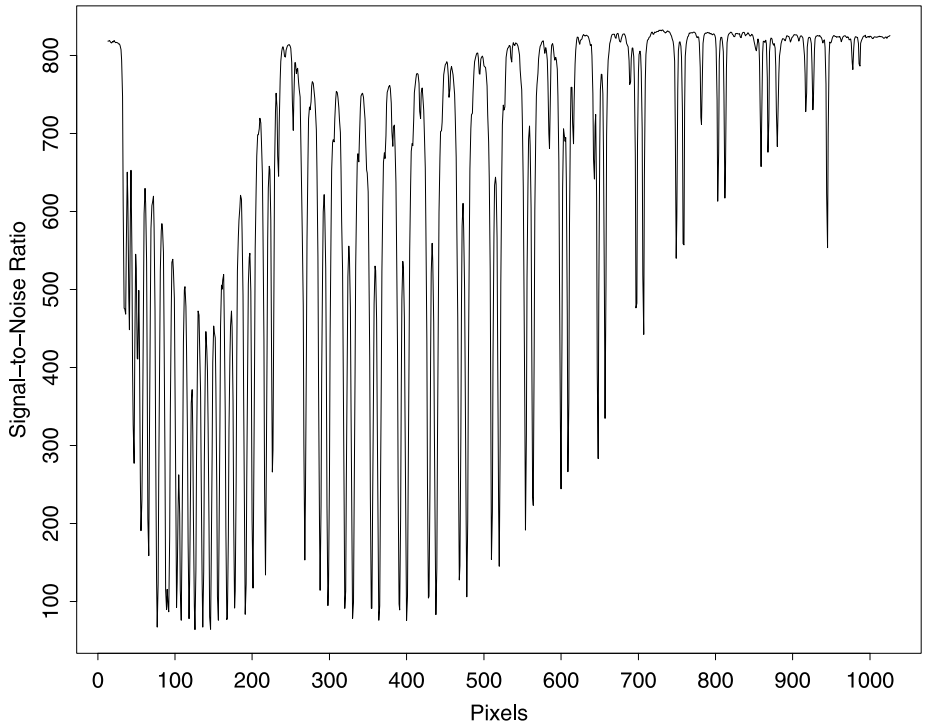

Figure 3. Estimated signal-to-noise ratio at 18:50 UTC on 20 June 2001.

20 June 2001 during 2 different sky conditions: clear sky and thick clouds. It is clear from the figure that the lines are individually resolved and that they have very large dynamic range, which is necessary for the retrieval of path length distribution as well as other applications. The wavelength registration is stable and accurate and the SNR is very high. The differences in the A-band and water vapor band spectra associated with aerosol (clear sky) and thick cloud conditions illustrate the presence of information content related to cloud optical and geometric properties.

2.2. Algorithm Development

[8] The discussion in the previous section emphasized that retrievals are very sensitive to slit function knowledge,

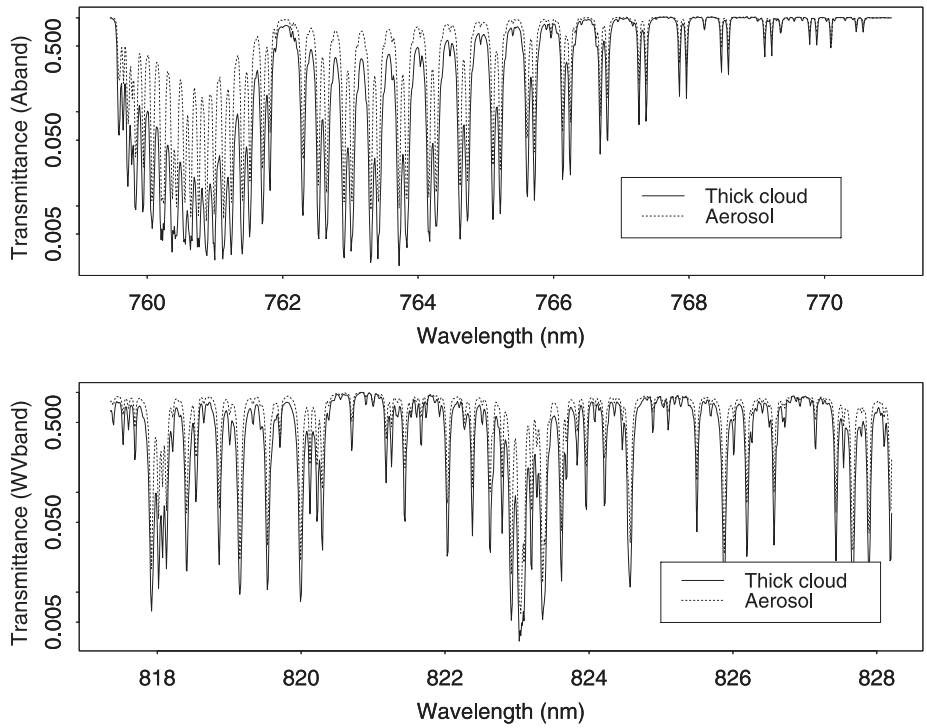

Figure 4. Measured spectra at oxygen A-band and 820 nm water vapor band at near local noon of 20 June 2001 at the ARM SGP site.

and that more information can be retrieved from higher resolution measurements. The critically important issue for high-resolution measurements is that since each pixel represents an integral over a distribution of absorption $\boldsymbol{k}$, the inversion kernel must contain accurate transmissions vs. path length data for these integrals. However, current measurements for slit function, solar spectrum and gaseous absorption spectra are not sufficiently accurate or congruent to allow the necessary accuracies in the needed transmission kernels. To avoid these problems, *Min and Clothiaux* [2003] have developed a new approach to infer photon path length distributions, by obtaining empirical calibration coefficients from direct-beam observations. The present work adopts this algorithm, but modifies it to apply to data from the HAWS; a brief description follows: For any measurement at a particular pixel,

$$\frac{I_p}{0} = \int_0^\infty S_p(k) \int_0^\infty P(l) e^{-kl}\, dl dk,$$

where $S_p(k)$ is the slit function for the p-th pixel, and P(l) is the photon path length distribution.

[9] For direct beam, $P(l) = \delta(\lambda - \lambda_0)$, for a particular path (a function of solar airmass or zenith angle), l_0. Since measurements from each pixel are convolved across both weak and strong absorption coefficients, the band model concept is adopted to deal with each pixel. The transmittance can be written by a simple polynomial-exponential function in terms of the generalized absorption coefficient. Therefore a transmittance model can be constructed from direct beam observation, e.g., integration over the slit function as a function of solar airmasses:

$$\frac{I_p^{dir}}{I_{p,0}^{dir}} = \int_0^\infty S_p(k) e^{-kl_0} dk = \sum_{i=0}^{2} \left(a_p^i + b_p^i s_w\right) \left(l_0 - l_{0,off}\right)^i \cdot e^{-\left(\alpha_p + a_p^1 s_w\right) l_0}.$$

The constants ai_p, b_p^i, α_p and α_p^i are determined by fitting direct beam measurements as a function of solar airmass for each pixel. The factor, s_w, represents the wavelength shift of the HAWS in oxygen A-band and 820 nm water vapor band. Because s_w is small the impact of wavelength drift on the transmittance model is assumed to be linear.

[10] The transmittance model is defined in such a way that after application the integrated slit function for diffuse measurement (the diffuse radiance) can be viewed as a simple Laplace transform of photon path length distribution. Because the inverse Laplace transformation is by itself an ill-posed problem and the retrieval depends upon it, we use a simple two-parameter gamma function to constrain the inversion [*Harrison and Min*, 1997]. As pointed out by *Min and Clothiaux* [2003], the choice of the gamma distribution was motivated by it being the actual photon path length PDF under optically thick cloud conditions. With the existence of the Laplace transform for gamma function and general shift operator for the Laplace transform (all photons must travel at least one atmosphere), an analytical model for retrieving photon path length distribution can be derived as *Min and Clothiaux* [2003],

$$\frac{I_p^{dir}}{I_{p,0}^{dir}} = \sum_{i=0}^{2} \int_0^\infty \left(l - l_{0,off}\right)^\beta e^{-\alpha(l - l_{0,off})} \left(a_p^i + b_p^i s_w\right) \left(l - l_{0,off}\right)^i \cdot e^{-\left(\alpha_p + \alpha_p^1 s_w\right) l} dl = \sum_{i=0}^{2} \left(\alpha_p^i + b_p^i s_w\right) \frac{\Gamma(\beta + i + 1)}{\left[\left(\alpha_p + \alpha_p^1 s_w\right) + \alpha\right]^{\beta + i + 1}} \cdot e^{-\left(\alpha_p + \alpha_p^1 s_w\right) l_{0,off}},$$

and the two parameters of the gamma function least squares regression from spectral measurements of diffuse radiance of the HAWS. Since both oxygen A-band and water vapor band are measured, the above formulations can be modified to infer the photon path length distributions inside both absorption bands. Furthermore, to acount for surface pressure variations, the photon path length is referenced to the standard atmosphere. In contrast to oxygen, the total column water vapor varies significantly. To deal with such variations, the column water vapor path (WVP) measurements observed by the microwave radiometer (MWR) is used, and we define $l = C_{wvp} l_n$.

3. Field Campaign at ARM SGP Site

[11] A field campaign was conducted at the ARM SGP site in Oklahoma during June 2001 to demonstrate the capabilities of HAWS and the retrieval algorithm described above. The ARM site is suited for this experiment because it is heavily instrumented to study clouds, aerosols and radiation transfer. Collocated passive and active radiometric instruments provide concurrent observations of cloud and aerosol optical properties and cloud geometric properties. For this study, cloud optical depth and effective radius of the droplet size distribution are simultaneously retrieved from surface measurements of the Multifilter Rotating Shadowband Radiometer and microwave radiometer (for liquid water path; LWP) using nonlinear least squares minimization in conjunction with an adjoint method of radiative transfer [*Min and Harrison*, 1996]. Cloud geometric and height information is determined from a zenith-pointing millimeter-wave cloud radar (MMCR [*Clothiaux et al.*, 2000]). Relative humidity profiles measured by a balloon-borne sounding system (BBSS) are also used to determine the cloud layer location and water vapor profiles.

[12] A special case observed on 21 June 2001 during the campaign is presented to demonstrate the potential of photon path length statistics derived from high resolution measurements of the HAWS to reveal information about cloud morphologies and water vapor absorption of solar radiation mediated by cloud effects.

[13] The retrieval for the present case is limited to two variables (mean and variance) only because of the limitation of the gamma distribution used. As discussed in Min and Harrison (submitted manuscript, 2003), the performance demonstrated by the HAWS should yield four independent pieces of information. Alternative constraints in the frame work of stochastic radiative transfer and truncated Levy-flight statistics are being explored to exploit the information

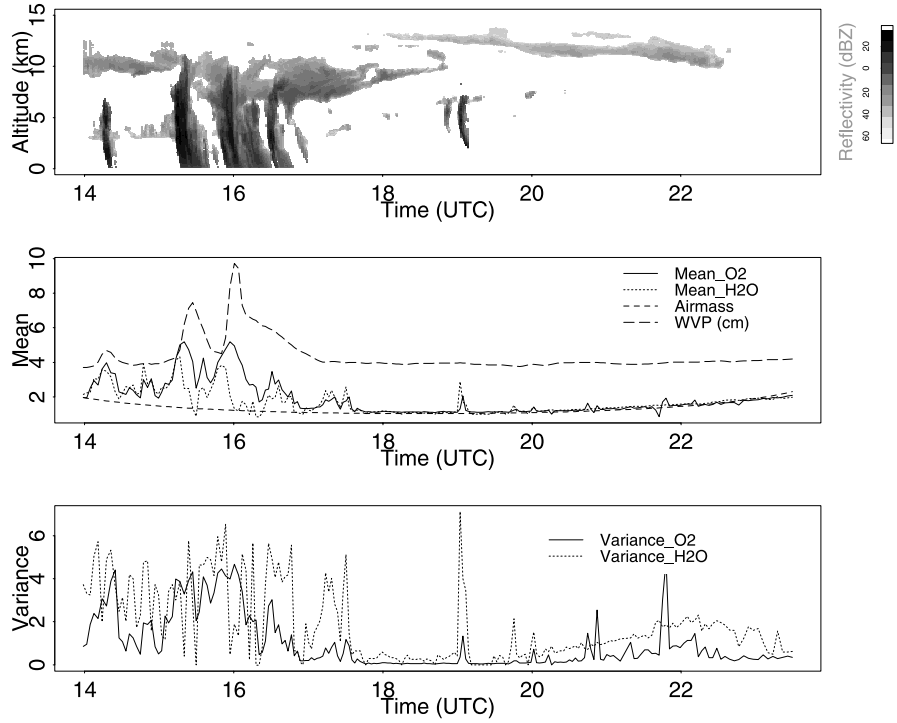

Figure 5. Cloud radar reflectivity, mean and variance of photon path length distribution retrieved from the prototype instrument at ARM SGP site on 20 June 2001.

content of measurements differently [*Su and Pomraning*, 1994; *Davis and Marshak*, 1997; *Pfeilsticker*, 1999].

[14] Reflectivity from the cloud radar (top panel of Figure 5) shows that four sky conditions occurred during the course of the day: multiple cirrus 14:00–15:30 UTC and 17:00–20:00 UTC; thick single-layer cloud 15:30–17:00 UTC; single-layer cirrus 20:00–22:30 UTC; and clear sky with aerosols 22:30–23:30 UTC. The inferred mean and variance of photon path length distribution in the A-band and at water vapor band are shown in the bottom two panels of Figure 5. The single-layer thick cloud and multiple-layer cloud periods (14–17 UTC) significantly enhance the distribution of photon path length and their corresponding variances while diminishing those inferred from the thin cirrus observations taken between (20–22 UTC). During the clear sky period (later afternoon), the mean path length is close to or slightly smaller that the airmass due to aerosol loading in the lower atmosphere. The results above are consistent with those from a moderate resolution A-band study using measurements from a Rotating Shadowband Spectrometer (RSS) [*Min et al.*, 2001]. In contrast to that instrument the HAWS measures zenith radiance and has a different FOV, which affects the interpretation and magnitude of the results, respectively. The mean path length and variance in the water vapor band show a corresponding enhancement for the observed sky conditions, but differ in shape and in magnitude from those of the A-band because unlike oxygen, there is considerable temporal and vertical variation of water vapor that is associated by the presence of clouds.

[15] Individual path length distributions inferred from observations during the cloudy and the clear sky periods are shown in Figure 6 to provide a more detailed picture of the effects of cloud morphology and impact of water vapor in contrasting conditions (in clouds or clear sky) on the characteristics and shape of the photon path length distribution. The path length distribution in the A-band observed at 15:34 during the thick and multiple layer cloud periods has a significantly enhanced mean and large variance due to scattering within the cloud and reflection between clouds. The mean (normalized) of the distribution in the water vapor band is also enhanced relative to that during the remaining 2 periods, but this enhancement is less than that in the A-band. This is because most of the water vapor resides at or below lower clouds, where photons are not subject to significant scattering as between or in clouds and thus accumulate much less water vapor absorption path than in the A-band. The A-band distribution at 20:00 UTC while the thin cirrus was present has a small mean path length ($\sim$1.1), which is close to one airmass. The closeness of the mean path length to one airmass is due to the altitude of the cirrus and to the absence of underlying clouds. The photons viewed by the sensor are scattered high in the atmosphere by the cirrus and, with no underlying clouds, they travel through a similar amount of oxygen as would a photon from the overhead sun in clear air, resulting in a path length that is similar to one airmass. The instrument field of view also reduces photons with longer path length. The difference between the mean A-band and mean water vapor band path length for the cirrus case is small because all photons travel through the total column amount of oxygen and water vapor. The variance is also small because there is a relatively small amount of aerosol in the clear atmosphere between the cirrus cloud and the sensor. Also contributing to the small variance is the negligible amount of multiple scattering that occurs in the thin cirrus. The mean of the

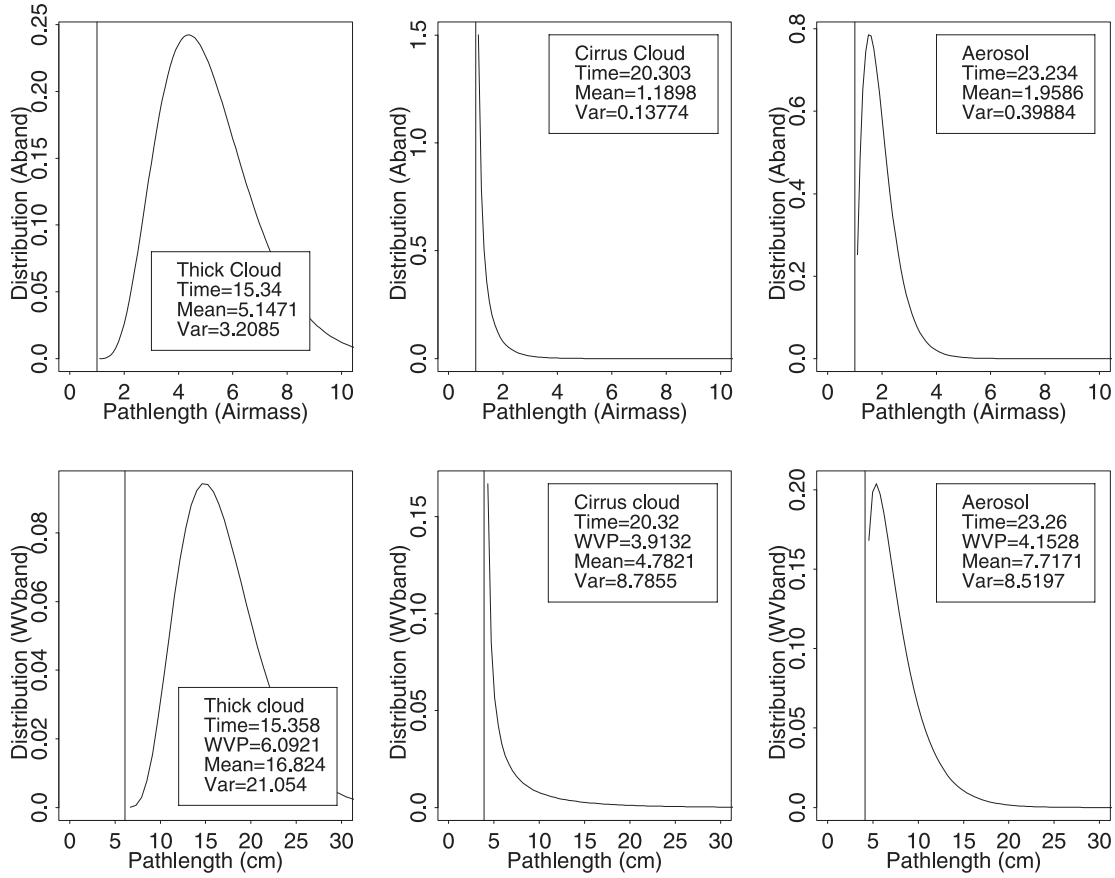

Figure 6. Photon path length distributions at oxygen A-band and water vapor band under thick cloud, thin cirrus cloud, and aerosol conditions during 20 June 2001.

A-band path length under clear sky conditions, 23:23 UTC, is also similar to the solar airmass. In this case the dominant scatters are aerosols, which are near the surface. Photons travel through most of the atmosphere before they are scattered by aerosols; therefore, the mean path length is almost the same as the solar airmass. Relatively thick aerosol loading results in moderate variance of the distribution as variance is sensitive to the thickness of the aerosol loading.

[16] Joint statistics for the four sky conditions identified above are shown in Figure 7 to further illustrate the impact of cloud morphology and sky condition on photon path length distribution and to also show the precision with which the relationship between variance and mean path length in both bands can distinguish different cloud geometries, aerosols and clouds conditions, and the location of water vapor in the vicinity of clouds. The left plot in the Figure 7 shows a scatterplot of the variance and mean of the path length distribution in the A-band, illustrating the correlation between the two. Clear sky cases represented by the letter "A" and thin cirrus cases, represented by "C" form a sort of lower and upper boundary, respectively, of all cases. The clear sky cases form the lower boundary; with only aerosol loading in the lower atmosphere the resulting variance is low and confined to 0.25–0.5, but with mean path length similar to the airmass for that period, range from 1.5 to 2.25. Thin cirrus cases also produce low variance and mean path length, but the variance extends over a wider range and the mean is confined to 1–2. Multiple- and thick-layer cloud cases, represented by "D" and "T" respectively, make up the cluster of points between the extremes of thin cirrus and clear sky in accordance with the substantially enhanced mean and variance produced by multiple- and thick-layer clouds.

[17] The mean-variance relationship of photon path length distribution in various sky conditions may be explained by photon diffusion theory. In a single-layer dense cloud system with fixed physical depth, the photon path length scales linearly with optical depth, illustrating characteristic of classical Brownian diffusion with Gaussian statistics [*Min et al.*, 2001]. For a multiple or complex cloud system, as shown here, a simple linear scaling is not seen. In the frame of photon diffusion theory, *Davis and Marshak* [2002] derived a mean-variance relation, $Variance = \frac{2}{5}(Mean - 1)^2$, for a homogeneous media. For the convenience of the reader this line is shown in the left panel of Figure 7. However, path lengths derived from A-band spectroscopy are intrinsically pressure and temperature weighted (where Davis and Marshak's discussion is geometric). Further, our moments are gamma constrained. Thus the quantities compared here are not identical. Nevertheless, this mean-variance curve with respect to a homogeneous model prediction provides a lower envelope on the observed data, demonstrating the bias of 1-D transmittances with respect to more complicated 3-D counterparts. The joint statistics provides an insight of radiative transfer process in the cloud system.

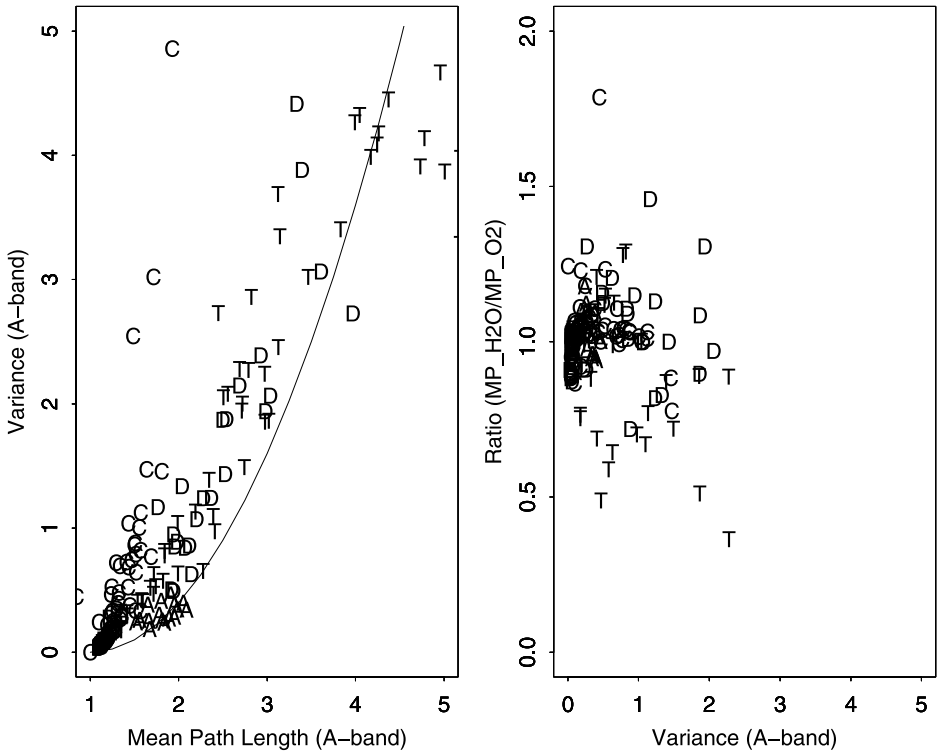

Figure 7. Joint statistics of mean and variance of photon path length at both oxygen A-band and water vapor band for four atmospheric conditions: multiple cirrus condition (D); thick cloud condition (T); single cirrus condition (C); and aerosol condition (A). The solid line represents theoretic prediction of mean-variance relationship.

[18] The right panel in the Figure 7 is a plot of the ratio of the mean path length in the water vapor band to that in the oxygen A-band versus the variance in the A-band. Features in this plot explicitly illustrate the ability of the HAWS system to provide accurate knowledge of the presence of water vapor in and between clouds, which is critical for understanding the cloud-water vapor interaction. For example, points associated with cases where the preponderance of oxygen and water vapor lie below and above the scattering layer (i.e., thin cirrus and aerosols in clear-sky, respectively) cluster about a ratio of one. For multilayer cirrus clouds and single-layer thick clouds, the ratio decreases with increasing variance in oxygen A-band, indicating that while the A-band path length is enhanced due to photons ricocheting between layers or inside thick clouds, the path length of photons at the water vapor wavelength remains small due to the lack of large amounts of water vapor between or inside the clouds present to cause significant scattering. These results are consistent with the findings of *Min and Clothiaux* [2003].

4. Summary and Conclusion

[19] A theoretical framework and prototype high resolution A-band and water vapor band spectrometer have been developed to study the applicability of photon path length statistics to the remote sensing of cloud and aerosol optical properties, effects of cloud geometry, and water vapor, particularly in the vicinity of clouds. The HAWS successfully achieved out-of-band rejection of better than 10^{-5}, a resolution of 0.5 cm^{-1}, and high signal-to-noise ratio, which are crucial to retrieval of atmospheric information through high resolution spectrometry in the A-band and water vapor band. A field campaign was conducted to demonstrate the capabilities of HAWS and the retrieval algorithm at the cloud and radiation testbed at ARM SGP site in Oklahoma, where a comprehensive set of radiometric, passive, and active sensors provide continuous and concurrent measurements of clouds, aerosols, water vapor, and other atmospheric properties. Results show that in the A-band, thick and multiple-layer clouds significantly enhance the mean and variance of the photon path length distribution. Thin high level cirrus produces relatively small mean distribution and variance, and mean path lengths comparable to or smaller than the solar airmass were associated with clear sky cases. The mean path length and variance in the water vapor band differs from that in the A-band due to the spatial inhomogeneity of water vapor amounts, particularly under cloudy conditions. Moreover, an analysis of joints statistics, the relationship between variance and mean path length in both bands, reveals the capability to detect the presence of water vapor between or in cloud layers. This may be very useful in the effort to better understand critical physical and radiative processes involved in the interactions between cloud and water vapor.

[20] The mean and variance of photon path length distribution when combined with the cloud optical depth and mean effective droplet radius provide a more comprehensive description of the optical properties of cloud systems.

Application of these parameters enable detection of some cloud and clear sky scenes which cannot be done readily by other passive remote sensing techniques, particularly the identification of cases where cloud layering or complex structure produces large photon path lengths. Most important is that the long-term climatology of these cloud properties can be used to test the extent to which GCM cloud-diagnostic schemes are realistic. It is valuable to combine photon path length PDF information from both the oxygen A-band and 0.820 μm water vapor band as doing improves understanding of how water vapor distribution and cloud morphology interact to affect absorption.

[21] Finally, based on information content analysis and as demonstrated by the performance of the HAWS, it should be possible to retrieve higher moments of photon path length distributions. Algorithms with other constraints will be explored in an attempt to provide useful alternatives and higher moments of photon path length distribution, and further investigations will be conducted to study the implications of joint statistics of the moments of photon path length distribution and optical depth on geometrical description of cloud overlapping and occurrence.

[22] **Acknowledgments.** This research was supported by the National Science Foundation under grant ATM-9973701 and by the Office of Science (BER), U.S. Department of Energy, Grants DE-FG02-03ER63531. Data were obtained from the Atmospheric Radiation Measurement (ARM) Program sponsored by the U.S. Department of Energy, Office of Energy Research, Office of Health and Environmental Research, Environmental Sciences Division.

References

Clothiaux, E. E., et al. (2000), Objective determination of cloud hights and radar reflectivities using a combination of active remote sensors at the ARM CART sites, *J. Appl. Meteorol.*, *39*, 645–665.

Davis, A., and A. Marshak (1997), Lévy kinetics in slab geometry: Scaling of transmission probability, in *Fractal Frontiers*, edited by M. M. Novak and T. G. Dewey, pp. 63–72, World Sci., River Edge, N. J.

Davis, A. B., and A. Marshak (2002), Space-time characteristics of light transmitted by dense clouds: A Green function analysis, *J. Atmos. Sci.*, *59*, 2713–2727.

Davis, A. B., R. F. Cahalan, J. D. Spinhirne, M. J. McGill, and S. P. Love (1999), Off-beam lidar: An emerging technique in cloud remote sensing based on radiative Green-function theory in the diffusion domain, *Phys. Chem. Earth, Part B*, *24*, 757–765.

Fischer, J., and H. Grassl (1991), Detection of cloud-top height from backscattered radiances within the oxygen A band. Part 1: Theoretical study, *J. Appl. Meteorol.*, *30*, 1245–1259.

Fischer, J., W. Cordes, A. Schmitz-Peiffer, W. Renger, and P. Morel (1991), Detection of cloud-top height from backscattered radiances within the oxygen A band: Part 2. Measurements, *J. Appl. Meteorol.*, *30*, 1260–1267.

Grechko, Y. I., V. I. Dianov-Klokov, and I. P. Malkov (1973), Aircraft measurements of photon paths in reflection and transmission of light by clouds in the 0.76 um oxygen band, *Atmos. Ocean Phys.*, *9*, 262–265.

Harrison, L., and Q.-L. Min (1997), *Photon Pathlength Distributions in Cloudy Atmospheres From Ground-based High-resolution O_2 A-band Spectroscopy, in IRS'96: Current Problems in Atmospheric Radiation*, edited by W. L. Smith and K. Stamnes, pp. 594, A. Deepak, Hampton, Va.

Heidinger, A., and G. L. Stephens (2000), Molecular line absorption in a scattering atmosphere: 2. Retrieval of particle properties, *J. Atmos.*, *57*, 1615–1634.

Houghton, J. T., et al. (2001), *Climate Change 2001*, Cambridge Univ. Press, New York.

Irvine, W. M. (1964), The formation of absorption bands and the distribution of photon optical paths in a scattering atmosphere, *Bull. Astron. Inst. Neth.*, *17*, 266–279.

Irvine, W. M. (1967), Absorption bands and photon optical paths in a nonconservative scattering atmosphere, *Astrophys. J.*, *147*, 1193–1197.

Liou, K. N. (1992), *Radiation and Cloud Processes in the Atmosphere*, Oxford Univ. Press, New York.

Love, S. P., A. B. Davis, C. Ho, and C. A. Rohde (2001), Remote sensing of cloud thickness and liquid water content with Wide-Angle Imaging Lidar (WAIL), *Atmos. Res.*, *59–60*, 295–312.

Min, Q.-L., and E. E. Clothiaux (2003), Photo path length distributions inferred from rotating shadowband spectrometer measurements at the Atmospheric Radiation Measurements Program Southern Great Plains site, *J. Geophys. Res.*, *108*(D15), 4465, doi:10.1029/2002JD002963.

Min, Q.-L., and L. C. Harrison (1996), Cloud properties derived from surface MFRSR measurements and comparison with GOES results at the ARM SGP site, *Geophys. Res. Lett.*, *23*, 1641–1644.

Min, Q.-L., and L. C. Harrison (1999), Joint statistics of photon path length and cloud optical depth, *Geophys. Res. Lett.*, *26*, 1425–1428.

Min, Q.-L., L. C. Harrison, and E. Clothiaux (2001), Joint statistics of photon pathlength and cloud optical depth: Case studies, *J. Geophys. Res.*, *106*, 7375–7386.

O'Brien, D. M., and R. M. Mitchell (1992), Error estimates for retrieval of cloud top pressure using absorption in the A band of oxygen, *J. Appl. Meteorol.*, *31*, 1179–1192.

Partian, P. T., A. K. Heidinger, and G. L. Stephens (2000), High spectral resolution atmospheric radiative transfer application of the modified equivalence theorem, *J. Geophys. Res.*, *105*, 2163–2177.

Pfeilsticker, K. (1999), First geometrical pathlength distribution measurements of skylight using the oxygen A-band absorption technique: 2. Derivation of the Lévy-Index for skylight transmitted by mid-latitude clouds, *J. Geophys. Res.*, *104*, 4101–4116.

Pfeilsticker, K., F. Erle, H. Veitel, and U. Platt (1998), First Geometrical pathlengths probability density function derivation of the skylight from spectroscopically highly resolving oxygen A-band observations: 1. Measurement technique, atmospheric observations and model calculations, *J. Geophys. Res.*, *103*, 11,483–11,504.

Portmann, R. W., S. Solomon, R. W. Sanders, and J. S. Danel (2001), Cloud moduation of zenith sky oxygen path lengths over Boulder, Colorado: Measurements versus model, *J. Geophys. Res.*, *106*, 1139–1155.

Stephens, G. L., and A. Heidinger (2000), Molecular line absorption in a scattering atmosphere: I Theory, *J. Atmos. Sci.*, *57*, 1599–1614.

Su, B., and G. C. Pomraning (1994), A stochastic description of a broken cloud field, *J. Atmos. Sci.*, *51*, 1969–1977.

van de Hulst, H. C. (1980), *Multiple Light Scattering. Tables, Formulas, and Applications*, vol. 1, Academic, San Diego, Calif.

Veitel, H., O. Funk, C. Kruz, U. Platt, and K. Pfeilsticker (1998), Geometrical path length probability density functions of the skylight transmitted by midlatitude cloudy skies: Some case studies, *Geophys. Res. Lett.*, *25*, 3355–3358.

J. Berndt, L. C. Harrison, P. Kiedron, and Q.-L. Min, Atmospheric Sciences Research Center, State University of New York, 251 Fuller Road, Albany, NY 12203, USA. (min@asrc.cestm.albany.edu)

E. Joseph, Department of Physics and Astronomy, Howard University, 2355 6th Street, N. W., Washington, DC 20059, USA.